AN EXPLOSIVE VOLCANIC ORIGIN IDENTIFIED FOR DARK SAND IN AEOLIS DORSA, MARS. D. M. Burr[1], C. E. Viviano[2], T. I. Michaels[3], M. Chojnacki[4], R. E. Jacobsen[5], [1]Department of Astronomy and Planetary Science, Northern Arizona University, Flagstaff, AZ, USA (Devon.Burr@nau.edu), [2]JHU Applied Physics Laboratory, [3]SETI Institute, [4]Planetary Science Institute, [5]University of Tennessee Knoxville.

Introduction: Aeolian sand has been a pervasive influence on Mars. Loose and lithified deposits are observed globally [1,2] and locally [3,4] and sand-abraded landforms record the erosional effectiveness of wind-driven sand over geologic time [5].

The primary origin(s) of these sand grains is(are) unknown [6]. This fundamental knowledge gap in our understanding of Martian source-to-sink sedimentology [2,7] is highlighted by detection of widespread dune movement today [8,9], during which the more-energetic impacts of saltating grain are inferred to break down those grains to sub-sand sizes [10]. Consistent with limited sand transport distances, local sand sources have been inferred [4] and lithified sand grains have been recycled [2,11]. However, the mechanism(s) that originated sand-sized grains remain(s) a key area of inquiry on Mars, as throughout the Solar System [6].

Multiple mechanisms might generate sand on Mars [12]. Volcaniclastic deposits, either explosive deposits or weathered lavas, are consistent with the low albedo and mafic signature of Martian dunes and a long-standing hypothesis for one origin of Martian sand [13].

Here, we test the volcaniclastic hypothesis within the Medusae Fossae Formation (MFF), interpreted as an ignimbrite [14-16]. The study area is the Aeolis Dorsa (AD; 0° - 8°S, 147.5° - 156°E) region (Fig. 1), named for its many inverted fluvial deposits [17] and showing erosional and depositional aeolian landforms. Yardangs (e.g., [5]), are pervasive and dark sand deposits are visible in yardang troughs (Fig. 2), as well as adjacent to topographic features and in Aeolis Chaos (Fig. 1C), a ~500-m-deep depression adjacent to the highlands.

Geologic mapping [17] and context (Fig. 1B) of the AD region enable testing of multiple volcaniclastic sources for this AD sand, namely from: i) the Elysium Mons edifice with its effusive and explosive deposits, ii) the effusive lavas of the Cerberus plains, iii) the intracrater sand of the southern highlands, and iv) the ignimbrite (MFF) plana units of the Aeolis Dorsa region. We evaluate each of these four regions as a possible source of the sand in Aeolis Dorsa.

Methodology: This evaluation of the possible source regions involved first mapping sand deposits in Aeolis Dorsa. We then developed expectations for sand composition and transport pathways from each region and compared those expectations to observations. Data from the Compact Reconnaissance Imaging Spectrometer for Mars (CRISM; [18]) were used to interrogate the mineralogies in the Cerberus Fossae, Elysium Mons, and southern highlands craters, comparing them to dark sand deposits in the AD region. Expectations for transport into and deposits in the study area were derived from potential sand flux modeling.

Results: Potential sand flux modeling shows limited transport into the AD area. Within AD, sand locations and potential transport imply sourcing from Zephyria Planum, a MFF deposit [17,19]. South of Zephyria Planum and within MFF yardang troughs, sand shows a uniquely olivine-rich signature (Fig. 1C), distinct from those of the three potential sand source regions external to AD (southern highlands, Elysium Mons, Cerberus plains). This distinctive olivine signature implies minimal mixing and/or transport from a local source.

Sand-generating mechanisms. Local sources for AD sand suggest a mechanism for sand genesis. Terrestrial basaltic ignimbrites can have native olivine sand-sized phenocrysts [20,21] and exhibit sand-rich layers tens of centimeters thick [22-24]. Thus, we examined images from the High-Resolution Imaging Science Experiment [25] on Plana units for dark sandy layers, finding 31 examples (Fig. 2A-C). CRISM data for one example demonstrates its olivine-rich mineralogy (Fig. 2D).

Implications: A pyroclastic source for plana sand, substantiating the volcaniclastic hypothesis, provides a mechanism for the global distribution of Martian sand from local sources. Pyroclastic deposits with sand-sized grains [26-28] have been inferred globally [19,29], identified regionally [30], and detected in situ [31]. The potential for sand saltation at moderate wind speeds [32,33] allows for further distribution. With the high grain impact velocities during low-density atmospheric conditions [34] over the past ~3 Gya, this abrasive sand generation likely operated over most of martian history.

Acknowledgments: This work was initiated at the University of Tennessee, on traditional territories of the Tsalagi (Cherokee), the Tsoyaha (Yuchi, Muscogee Creek), and other Native peoples. It was completed at the Northern Arizona University on homelands sacred to Hohokam Diné, Hopi, Western Apache, and other Native peoples. We honor these tribes on their ancestral lands. This work was supported by NASA grant NNX16AL47G via the Mars Data Analysis Program.

References: [1] Hayward R. K. et al. (2014) *Icarus 230,* 38-46. [2] Grotzinger J.P. and Milliken R. E. (2012) *SEPM Spec. Pub.* 102. 1-48. [3] Rampe E.B. et al. (2017) *GRL 45*, 9488-9497. [4] Diniega S. et al. (2021) *Geom. 380*, 107627. [5] Ward A.W. (1979) *JGR 84,* 8147-8166. [6] Fenton L.K. et al. (2013) *Aeolian*

Res. 8, 29-38. [7] Kocurek G.A. and Ewing R.C. (2012) *SEPM Spec. Pub. 102*, 151-168. [8] Bridges N.T. et al. (2012) *Nat. 485*, 339-342. [9] Chojnacki M. et al. (2019) *Geol.* doi.org/10.1130/G45793.1. [10] Sagan C. et al. (1977) *JGR 82*, 4430-4438. [11] Edgett K.S. et al. (2020) *Geosphere 16*, 1508-1537. [12] Greeley R. and Iversen J.D. (1985) *Wind as a Geological Process.* [13] Edgett K.S. and Lancaster N. (1993) *J Arid Env. 25,* 271-297. [14] Kerber L. et al. (2011) *Icarus 216,* 212-220. [15] Mandt K.E. et al. (2008) *JGR 113,* E12011. [16] Watters T.R. et al. (2007) *Sci. 318*, 1125-1128. [17] Burr D.M. et al. (2021) *USGS SIM 3480*. [18] Murchie S. et al. (2007) *JGR 112,* E05S03. [19] Tanaka K.L. et al. (2014) *USGS SIM 3292*. [20] Clemens J.D. et al. (2011) *Contrib. Min. Petrol 162*, 1315–1337. [21] Martí J. et al. (2017) *Bull. Volc. 79,* 33. [22] Fisher R.V. et al. (1993) *JVGR 56,* 205-220. [23] Scarpati C. et al. (2015) *Bull. Volc.. 77,* 97. [24] Valentine G. et al. (2019) *Bull. Volc. 81*, 29. [25] McEwen A.S. et al. (2007) *JGR 112,* E5. [26] Hynek B.M. et al. (2003) *JGR 108,* E9, 5111. [27] Wilson L. and Head J.W. (1994) *Rev. Geophys. 32*, 221-263. [28] Kerber L. et al. (2012) *Icarus 216,* 358-381. [29] Broz P. et al. (2021) *JVGR*, 107125. [30] Kremer C.H. et al. (2019) *Geol. 47,* 677-681. [31] McCoy T.J. et al. (2008) *JGR 113*, E06S03. [32] Sullivan R. and Kok J.F. (2017) *JGR 122*, 2111-2143. [33] Andreotti B. et al. (2021) *PNAS* 118, e2012386118. [34] Kok J.F. et al. (2012) *Rep. Prog. Phys. 75*, 106901.

Fig. 1: A) Context image with MFF (outlined in red), location of panel B (white box). B) Regional view of the four possible sand source regions with mineral identifications. Areas within by fuzzy black line indicate CRISM data for each region. C) AD study area in shaded relief with plana units (tan [17]), mineral identifications (as on B), sand (pale green) and sand-rich areas (blue boxes).

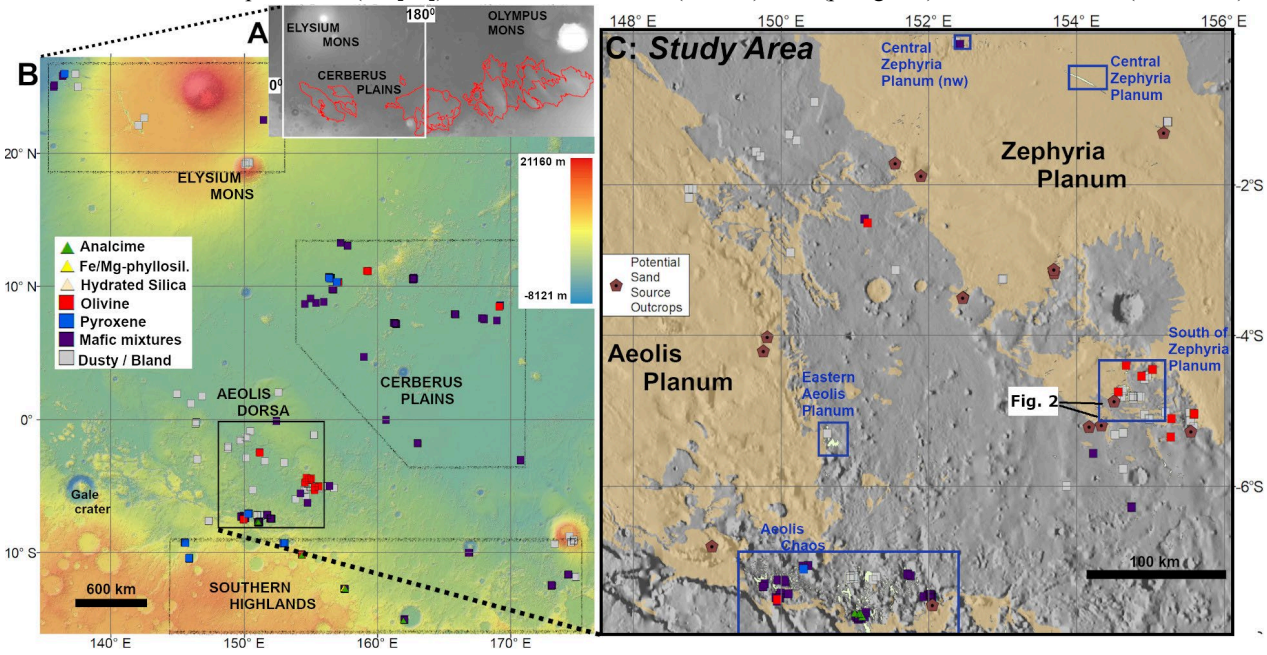

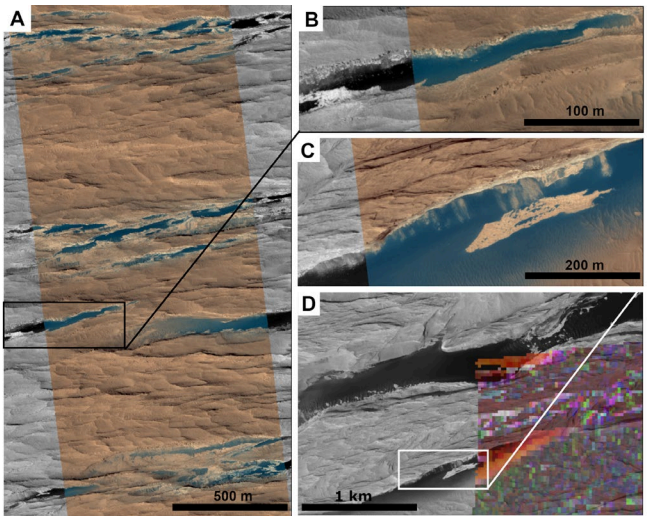

Fig. 2: Examples of sand source outcrops south of Zephyria Planum (location shown on Fig. 1C).
A) Several sand source outcrops in HiRISE image ESP_048246_1750_MRGB. The location of panel B is outlined in black.
B) A sand source outcrop shown in panel A.
C) A sand source shown in HiRISE image ESP_048747_1750_MRGB.
D) Outcrop in panel C overlain by CRISM data from cube FRS0003977D with R: BDI1000VIS, G: BD1300, B: BDI1000IR; red-orange tone coincides with olivine-enriched material. White box indicates location of panel C.